Technical Document 2516
December 1992

Application of the Finite-Difference Time-Domain Method to Scattering and Radiation Problems Involving Wires and Plates

B. Beker
College of Engineering
University of South Carolina

Technical Document 2516
December 1992

Application of the Finite-Difference Time-Domain Method to Scattering and Radiation Problems Involving Wires and Plates

B. Beker
College of Engineering
University of South Carolina

NAVAL COMMAND, CONTROL AND OCEAN SURVEILLANCE CENTER
RDT&E DIVISION
San Diego, California 92152–5001

J. D. FONTANA, CAPT, USN
Commanding Officer

R. T. SHEARER
Executive Director

ADMINISTRATIVE INFORMATION

This work was performed by the University of South Carolina under the 1992 ASEE-US Navy summer Faculty Research Program at the Naval Command, Control and Ocean Surveillance Center, Research, Development, Test and Evaluation (RDT&E) Division, Code 824, San Diego, CA 92152–5000.

This document partially fulfills Milestone 2, Task Number 2 (Total Ship Considerations) of the Electromagnetic Compatibility Project (RH21C13) of the Surface Ship Technology Block Program (PE0602121N). The work was sponsored by the Office of Naval Technology, currently renamed the Office of Naval Research.

Released by
J. B. Rhode, Head
Electromagnetic Technology
and Systems Branch

Under authority of
R. J. Kochanski, Head
Communications Systems
Engineering and
Integration Division

ACKNOWLEDGMENT

The author wishes to thank J. C. Logan for many helpful discussions regarding the numerical results appearing in this report, and J. H. Schukantz for sharing his practical expertise on time-domain scattering as well as for measured data on NRaD's time-domain range. The author also wishes to express his appreciation to Linda Russell and Pete S. T. Li for their very useful suggestions. Finally, the author thanks the entire staff of Code 82 for making him welcome at NRaD during the course of this research.

PK

CONTENTS

FIGURES

1.0 INTRODUCTION

Numerical modeling of electromagnetic (EM) interaction is normally performed by using either differential or integral equation methods. Both techniques can be implemented to solve problems in frequency or time domain. The method of moments (MOM) approach (Harrington, 1968) to solving integral equations has matured to the point where it can be used to solve complex problems. In the past, MOM has only been applied to scattering and radiation problems involving perfectly conducting or isotropic penetrable, lossy or lossless objects. However, many materials, (e.g., composites that are used on the Navy's surface ships in practical applications) exhibit anisotropic properties. To account for these new effects, several integral equation formulations for scattering and radiation by anisotropic objects have been developed recently (Graglia & Uslenghi, 1987; Monzon, 1988; Beker et al., 1989). Their applications were reviewed in a recent report by Beker (1992).

The differential equation approach to EM interaction studies has seen the emergence of the finite-difference time-domain (FD-TD) method (Yee, 1966) as the method of choice in many of today's scattering and radiation applications. This approach has been applied to study transient as well as steady-state scattering from many complex structures, radiation from wire antennas, and coupling into wires through narrow apertures in conducting cavities (Taflove, 1988). Because this method is volumetric in nature, it can treat conducting or penetrable media with equal effectiveness. As a result, in addition to isotropic media, FD-TD can predict EM response from inhomogeneous or anisotropic objects without any changes to the basic algorithm.

It is important to determine whether or not, and how effectively, the FD-TD can be used to solve EM interaction problems of interest to the Navy, such as investigating potential EM interference in shipboard communication systems. Consequently, this report partly addresses this issue by dealing exclusively with FD-TD modeling of time-domain EM scattering and radiation.

There are several existing general purpose FD-TD codes that have been written and used to analyze large- and small-scale EM interaction problems. The code developed by the Lawrence Livermore National Laboratory (LLNL), called the temporal and scattering response (TSAR) code (McLeod, 1990,1992), was made available to NRaD as well as to the University of South Carolina for evaluation during the course of this work. The objectives of the TSAR evaluation were to see how easy it was to use and whether or not it can help in numerical modeling of transient EM effects resulting from scattering and radiation in a complex EM environment, (e.g., the topsides of Navy surface ships).

2.0 FINITE-DIFFERENCE TIME-DOMAIN (FD-TD) METHOD FOR EM INTERACTION PROBLEMS

This chapter provides an introduction and evaluation of the LLNL's FD-TD software (McLeod, 1990), called TSAR, and its associated utilities (modules). First, a brief description of the FD-TD method is provided to familiarize the user with the minimum knowledge of the method that is needed to use TSAR properly. An overview of the entire TSAR software that summarizes how its various modules are interrelated is also included.

2.1 BRIEF OVERVIEW OF FD-TD

The FD-TD method is a very powerful technique for modeling TD interaction of EM fields with their surroundings. The method's greatest strength is its volumetric nature, which makes the FD-TD capable of simulating complex geometries and inhomogeneous materials. Due to this inherent generality, the method requires more computer resources than the surface integral equation techniques. However, with rapidly advancing modern computer technology, the resource issue is becoming less significant.

The validity of the method has been well established for scattering, radiation, and guided-wave-propagation problems. FD-TD has already been used to solve many different problems, including those that are of interest to the Navy. A recent study was reported on use of FD-TD to investigate EM field penetration into the bridge of a ship (Kashyap et al., 1992). This study demonstrated the feasibility of using FD-TD to investigate the coupling of incoming EM signals into electronic components located on the bridge. The results point to the need to further explore the capabilities of the FD-TD method for modeling shipboard antennas, protecting sensitive electronic equipment from external radiation, as well as other EM compatibility issues on Navy surface ships.

The following discussion concentrates on highlights of FD-TD. The basic knowledge of this method is required for anyone using available FD-TD computational packages such as TSAR to solve EM interaction problems. Although the numerous sources detail the method at length, the interested reader is referred to Taflove (1988).

To illustrate the basic idea behind FD-TD, the differential equation for the z-component of the electric field will be considered. According to Ampere's law, the electric and magnetic fields are related as

$$\frac{\partial E_z}{\partial t} = \frac{1}{\varepsilon}\left(\frac{\partial H_y}{\partial x} - \frac{\partial H_x}{\partial y} - \sigma E_z\right) \tag{1}$$

where ε and σ are the permittivity and conductivity, which can vary from point to point in space. In Cartesian coordinates, the space derivatives can be approximated by finite differences. This discretization of space and the location of field components can be best described graphically (figure 1) by the Yee cell (Yee, 1966).

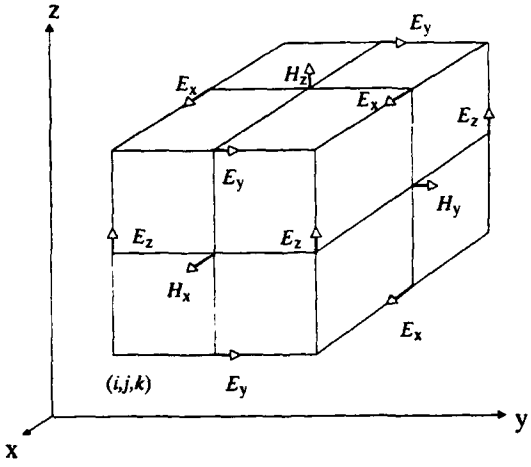

Figure 1. The Yee cell.

Notice that on every face of the lattice cube, the components of the electric field are looping or circulating around components of the magnetic field. This, in effect, simulates one of Maxwell's curl equations, namely Faraday's law. A similar picture can also be obtained for Ampere's law by simply displacing the Yee cell by one-half of the cell dimension. The resulting picture will then show the magnetic field circulating around components of the electric field.

Applying finite differences in time and space to equation (1) leads to the following approximation for E_z

$$E_z^{n+1}(i,j,k+1/2) = \frac{1-\dfrac{\sigma(i,j,k+1/2)\Delta t}{2\varepsilon(i,j,k+1/2)}}{1+\dfrac{\sigma(i,j,k+1/2)\Delta t}{2\varepsilon(i,j,k+1/2)}} E_z^n(i,j,k+1/2)$$
$$+\frac{\Delta t}{\varepsilon(i,j,k+1/2)}\left[1+\frac{\sigma(i,j,k+1/2)\Delta t}{2\varepsilon(i,j,k+1/2)}\right]^{-1}$$
$$\times\left\{\frac{H_y^{n+1/2}(i+1/2,j,k+1/2)-H_y^{n+1/2}(i-1/2,j,k+1/2)}{\Delta x}\right.$$
$$\left.+\frac{H_x^{n+1/2}(i,j-1/2,k+1/2)-H_x^{n+1/2}(i,j+1/2,k+1/2)}{\Delta y}\right\}. \qquad (2)$$

It is important to observe that both the permittivity and conductivity in equation (2) are specified at the same location as is the z-component of the electric field. The same is also true for E_x and E_y. This means that the electric properties of any medium in the volume modeled by FD-TD must be associated with the components of the electric field. Due to the symmetry between Faraday's and Ampere's laws, this also implies that the magnetic properties of various media under consideration must be associated with the components of the magnetic field. This becomes important when data must be specified to FD-TD solvers like TSAR; otherwise erroneous results will be obtained. More will be said in the subsequent discussion of the TSAR software.

Since the FD-TD method is used to advance field evolution in time, the time-stepping algorithm must be stable. Specifically, it must satisfy causality, which is ensured when the Courant stability condition is satisfied. In Cartesian coordinates, this condition is given by

$$c_{max}\Delta t \leq \left\{\frac{1}{(\Delta x)^2}+\frac{1}{(\Delta y)^2}+\frac{1}{(\Delta z)^2}\right\}^{-\frac{1}{2}}, \tag{3}$$

where C_{max} is the maximum phase velocity of a wave propagating in the medium under consideration.

Unlike the integral equations, FD-TD is based on the numerical solution of partial differential equations, which do not provide for natural boundary truncation. To simulate the field behavior at infinity close to the region of interest where EM interaction is taking place, absorbing boundary conditions must be employed. This allows for having a finite volume of space that needs to be modeled on a computer using its finite resources. The most common absorbing boundary conditions (ABCs) used for FD-TD are based on wave equation factoring (Mur, 1981). However, the factoring is intended to absorb only outgoing waves, namely waves that are incident on the plane (or absorbing boundary) at which these ABCs are applied.

In FD-TD, the ABCs are implemented by subdividing the entire computational lattice into two distinct zones (figure 2). One zone, where the object is located, contains the total fields; while in the other zone, incident fields are subtracted from the total fields. Hence, the scattered field zone contains only the outgoing waves that can be numerically absorbed using the available ABCs. Normally, the scattered field zone is only several space cells wide. However, if made too small, the imperfection due to ABCs will couple into the total field zone and produce nonexistent excitation to the region of interest.

In addition to providing the means for generating outgoing waves that are required for effective numerical simulation of radiation boundary conditions, the zoning also allows for natural generation of the excitation to the problem (Taflove, 1988; Taflove & Umashankar, 1987). The plane wave must be added (or subtracted) at the zone boundary to maintain consistency in the finite-difference approximation of spatial derivatives in the curl equations on each side of the zone. In other words, alike quantities must be added (or subtracted) as the total/scattered field boundary is crossed by the algorithm.

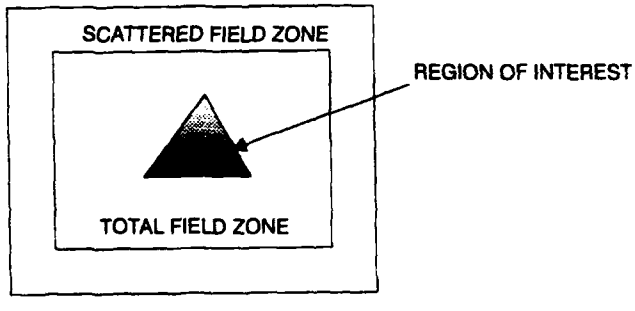

Figure 2. Total/scattered field zone for enforcing ABCs and introducing the excitation.

To complete the overview of FD-TD, it is important to discuss the mechanism for far-field calculation. In their most common form, FD-TD algorithms are employed to study near-field interaction only. In order to obtain far-field information by using the same approach as for the total fields while in the vicinity of the scatterer, a very large computational lattice is required. This technique is unnecessary if integral equations and the equivalence theorem are used instead. For steady-state far-fields, this approach requires a virtual surface that totally encloses the scatterer in the region of interest. Total fields are calculated on this surface and then are used as equivalent sources to obtain the corresponding far-fields (Umashankar and Taflove, 1982). The same can also be accomplished directly in the time domain. However, in this case, transient equivalent currents are used as sources for the far-field in integral equations cast in the time domain (Luebbers et al., 1991).

Like any other numerical method, FD-TD has some artifacts associated with various numerical approximations. Since finite differences are used to replace derivatives, the spatial resolution of the volume occupied by the object being modeled must be sufficiently fine to keep the higher order terms small. Typical resolution should be at least 10 cells per wavelength. This criterion minimizes numerical dispersion that can affect the speed of propagation of the field in different directions. A good practice in setting up the FD-TD problem is not to have an unnecessarily large number of cells in regions where no objects are present, thus avoiding field propagation over empty grids.

2.2. OVERVIEW OF THE LLNL's TSAR CODE AND SUPPORT UTILITIES

The LLNL's TSAR code is a general purpose FD-TD computational engine. Generality is TSAR's greatest strength as well as its greatest weakness. It can solve a lot of different problems at the same time that it becomes an "overkill." TSAR distribution comes with several support utilities that play a key role in making it work. Version 2.3 of TSAR was used in this evaluation. With this version, scattering as well as radiation problems can be analyzed. The present limitations of the code include the stepped-edge approximation to curved surfaces only.

For TSAR to work properly, several preprocessing utilities have to be employed. Specifically, TSAR needs a solid body generating program, multidevice graphics editor (MGED) developed by the Ballistic Research Laboratory (BRL) (Applin et al., 1988). MGED creates the object or group of objects that the user wants to analyze by using FD-TD. At this stage, such information as the shape, size, and material properties of the object that is to be modeled by TSAR are generated and stored into a file with *.*g* extension.

However, TSAR cannot use this information directly. The output file that was built with MGED has to be interpreted by another LLNL supplied utility called Anastasia or ANA (Laguna, 1990). The primary function of ANA is to create a mesh (or a finite-difference grid) for TSAR, so that the FD-TD solver can be used to study interaction of the generated object with external or internal EM fields. ANA performs additional functions such as specifying the types of the absorbing boundary conditions or allocation of padding cells that separate the object from the truncation boundary. The output of ANA is subsequently stored into an ASCII file having the *.*cla* extension.

Following the meshing of the solid body model, though not required for running TSAR, the user should always check to see if meshing was performed correctly. This can be done by using the IMAGE utility (McLeod and Allison, 1990) that graphically displays the geometry (output from ANA) that will be passed along to TSAR. The information is displayed in the form of colored lines corresponding to the electric/magnetic field components. The 16 available colors denote the 16 different materials that the user can specify in creating the object with MGED. At the present time, this places an upper limit on how many different material types can be used to compose an object or objects for a single problem.

To complete the problem specification to TSAR, the user needs to create and provide three additional ASCII input files *params.inc, projprms.inc,* and *tsarin*. MGED, ANA, and IMAGE utilities only deal with the geometry aspect of the overall input to TSAR. The purpose of *parms.inc,projprms.inc,* and *tsarin* files is to specify the lattice size, type of excitation, duration of TSAR run, and locations where near and far fields, as well as current densities, should be recorded. Creation of *params.inc*, *projprms.inc*, and *tsarin* files constitutes the end of input data preprocessing (figure 3). Note that creation of these files can be simplified using TSAR's command-driven `setup_tsar` utility.

As mentioned above, the three ASCII files, *params.inc*, *projprms.inc*, and *tsarin*, are required to inform TSAR of what is to be done. The best way to explain what these files mean is by example. Consider copies of *params.inc* and *tsarin* that come with TSAR distribution and are located in a directory *tsar/examples/monopole/input*. First, here is a sample of the *params.inc* file for a grounded, 30-cm-long conducting monopole that is excited by a plane wave.

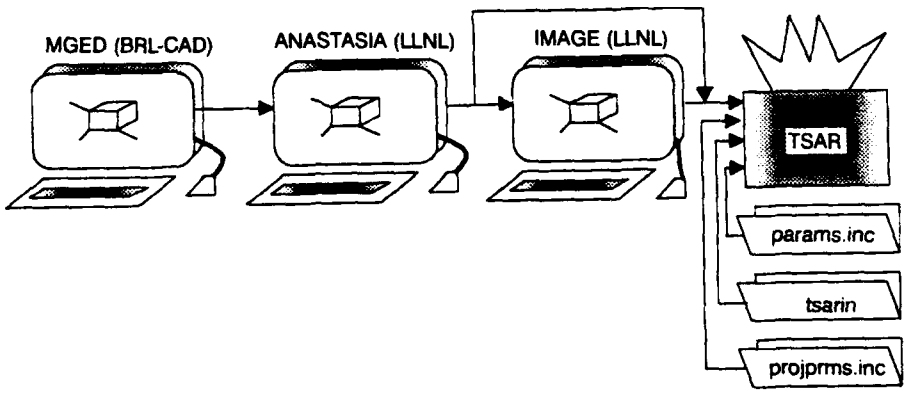

Figure 3. The entire TSAR system.

```
c=============================================================================c
c                                                                             c
c     USER-DEFINABLE PARAMETERS FOR TSAR                                      c
c                                                                             c
c                                                                             c
c     MaxI        Number of cells in the I direction                        c
c     MaxJ        Number of cells in the J direction                        c
c     MaxK        Number of cells in the K direction                        c
c     JBufSize    J planes in core memory                                   c
C     MaxPnt      Maximum # of point field sensors                          c
c     MaxRad      Maximum # of internal radiators                           c
c     MaxTime     Maximum length of user-supplied pulses                    c
c     MaxUser     Maximum # of user-supplied pulses                         c
c     MatlBits    Number of bits for each material index                    c
c     MaxSlice    Maximum # of Slice sensors                                c
c     Maxvol      Maximum # of Volume sensors                               c
c     InpFile              Name of name-list user input file                c
c=============================================================================c

      PARAMETER ( MaxI     =          60)
      PARAMETER ( MaxJ     =          40)
      PARAMETER ( MaxK     =          60)
      PARAMETER ( JBufSize =          40)
      PARAMETER ( MaxPnt   =          20)
      PARAMETER ( MaxRad   =          20)
      PARAMETER ( MaxTime  =        4096)
      PARAMETER ( MaxUser  =           4)
      PARAMETER ( MatlBits =           3)
      PARAMETER ( MaxSlice =          10)
      PARAMETER ( Maxvol   =          10)
      PARAMETER ( InpFile  =      'tsarin')
```

Notice that in this file, all parameters, for the most part, are self-explanatory. More detailed explanations, if needed, are available in the LLNL provided users' manuals (McLeod, 1990; 1992). The most critical input data in this file are the `MaxI`(`J` or `K`), `MaxTime`, and `InpFile`, which tells the TSAR the size of the lattice (computational space), how long it should run, and where it can find the rest of the input.

Next, consider the *tsarin* file for the same monopole example that is reproduced below:

```
$INPUT
Title = '30 cm monopole, shorted, 1/9/90'
NSteps = 512
ConductE(2) = 5.8E7
ConductE(3) = S.8E7
GridFile = 'monopole.cla'
Dx = .01
PeakTime = 30
PntX(1) = 30
PntY(1) = 0
Pntz(1) = 30
PntType(1) = 'CURRDENS'
PntDirY(1) = 1
PntDirZ(1) = 0
```

```
BCXMin = '2nd order Mur'
BCXMax = '2nd order Mur'
BCYMin = 'Electric Perfect Conductor'
BCYMax = '2nd order Mur'
BCZMin = '2nd Order Mur'
BCZMax = '2nd Order Mur'
ScatlMin = -1
FlagExtn = .TRUE.
FlagVrfy = .TRUE.
FlagEcho = .TRUE.
Theta = 90.
Phi = 180.
Polar = 0.
$END
```

This file informs TSAR that transient scattering by a grounded, 30-cm-tall copper monopole excited with a Gaussian plane wave pulse that peaks at 30 Dt and is 8 Dt wide should be modeled. Observe that the time waveform of the excitation is not explicitly stated in either *params.inc* or in *tsarin*. It is the default setting, as mentioned in the LLNL user's manual (McLeod, 1990, pp. 9, 10).

The *tsarin* file also contains the information regarding the kind of absorbing boundary conditions, field probe type, and customized adjustments for the location of the total/scattered field zone. Lattice truncation boundaries can be of several kinds: perfectly conducting electric or magnetic planes, as well as ABCs numerically simulating the radiation boundary conditions. The BCx(Y or Z)M(ax or in) are the parameters that tell TSAR what these conditions are. By default, the total/scattered field zone boundary is located four space cells away from the lattice boundary. The user may move this boundary closer to or farther away from the outer lattice planes by adjusting the scatx(Y or Z)M(ax or in) parameters.

Observe that, in this case, the point sensor type PntType is CURRDENS, which tells TSAR to compute the current density at a specified location. Using the HFIELD point sensor on the wire to compute the tangential *H*-field will *not* produce induced current density. This is because the magnetic field is calculated by TSAR one-half space cell away from the wire, whereas the CURRDENS probe interpolates between several *H*-field values near the wire to estimate the current density. As a result, if penetrable structures are being analyzed, then a very fine discretization is required to obtain accurate values of the magnetic or electric surface fields.

As mentioned earlier, the geometry is passed to TSAR in a form of an ASCII file created with MGED and meshed with ANA. For the monopole example, this file, called *monopole.cla*, is shown below.

```
# STPs 30cm shorted monopole on a ground plane
#
ascii
# Time sequence
time                          0.000000
float_precision               32
int_precision                 32
dependent_values              3
```

```
dependent_value-type          0 0 Ex
dependent_value-type          1 0 Ey
dependent_value-type          2 0 Ez
dependent_value-range         0 0 16
dependent_value-range         1 0 16
dependent_value-range         2 0 16
ordering                      0
res_x                         60
rest                          40
res_z                         60
delta_x                       10.000000
delta_y                       10.000000
delta_z                       10.000000
origin_x                      -300.000000
origins                       0.000000
origin_z                      -300.000000
grid_dimension                3
grid_type                     1
grid_data                     30


30  0 30 0 3 0
30  1 30 0 2 0
30  2 30 0 2 0
30  3 30 0 2 0
30  4 30 0 2 0
30  5 30 0 2 0
30  6 30 0 2 0
30  7 30 0 2 0
30  8 30 0 2 0
30  9 30 0 2 0
30 10 30 0 2 0
30 11 30 0 2 0
30 12 30 0 2 0
30 13 30 0 2 0
30 14 30 0 2 0
30 15 30 0 2 0
30 16 30 0 2 0
30 17 30 0 2 0
30 18 30 0 2 0
30 19 30 0 2 0
30 20 30 0 2 0
30 21 30 0 2 0
30 22 30 0 2 0
30 23 30 0 2 0
30 24 30 0 2 0
30 25 30 0 2 0
30 26 30 0 2 0
30 27 30 0 2 0
30 28 30 0 2 0
30 29 30 0 2 0
end_grid_data
end_time
```

This file illustrates how TSAR interprets the object geometry and its material properties in relation to the discretized Maxwell's curl equations such as, for example, equation (2). Most important are rows of numbers corresponding to the location of the dipole and its medium description. Recall that medium characteristics are assigned to the same locations within the lattice where the fields are specified. By default, the entire computational space is assumed to be occupied by free space. Hence, anything other than free space has to be specified at the input stage.

When the *monopole.cla* file is read, TSAR scans to see what the structure is. In addition to the other information contained in this file, the `grid_data = 30` indicates that the following 30 lines contain information corresponding to the wire. Data are interpreted by reading the location of the cell whose material characteristics at this lattice point are different than those of free space (first three numbers of each row). Then, the next three numbers correspond to the material properties assigned to x-, y-, and z-components of the electric field (last three numbers of each row). For the case of the monopole with a 1 x 1 cm square cross-section, it is sufficient to assign the conductivity to one component of the E-field only. If, on the other hand, the cross-section of the monopole were several cells thick, then the conductivity would have to be assigned to other components of the electric field as well. ANA does this automatically once the solid body file for this structure is available. Similarly, magnetic material objects can be modeled by assigning their relative permeability values to the appropriate components of the magnetic field.

Once the geometry of the problem is created by MGED, interpreted by ANA, checked with IMAGE, and fed to TSAR along with *params.inc, projprms.inc*, and *tsarin*, TSAR can provide a great deal of information for the user. At the present time, TSAR writes the point sensor data to ASCII files in a SIGEX format (McLeod 1992), by default called *point01, point02*, ..., etc. (figure 4). Typically, these are the field values computed at every time step.

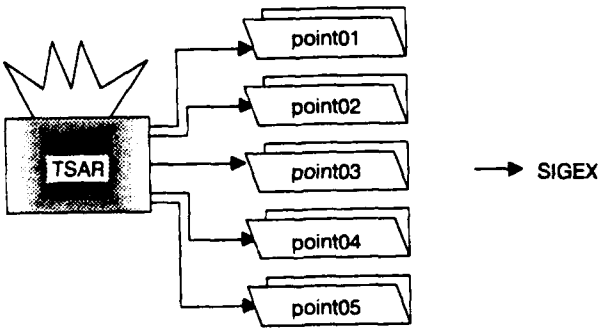

Figure 4. Output mode of TSAR.

Finally, a word of caution. TSAR is adapted for use on computers with UNIX operating systems. As a result, TSAR and its support software (MGED, Image, and Anastasia) are susceptible to changes or updates in operating systems. It is possible for TSAR not to work properly when the operating system is upgraded. In this case, it will have to be reinstalled along with the new OS. TSAR, however, is robust and seems to handle changes rather well, as shown when it was

tested and optimized on computers at LLNL. For example, with the tested distribution version, TSAR came to NRaD optimized for the Silicon Graphics IRIS 4-D workstation, but was never installed nor tested on the Convex computer at LLNL. As a result, it ran up to four times faster on the IRIS than it did on the Convex.

2.3 OVERVIEW OF BRL SOLID BODY MODELER

The MGED is a powerful tool for creating arbitrary solid objects. Development of the MGED started in 1980 at the Army's Ballistic Research Laboratory (BRL), and is still continuing (Applin et al., 1988, 1991). The strength of this solid body modeler (often referred to as BRL-CAD) is its graphical user interface. The graphical data input and output capability of MGED simplifies creation and editing of complex structures such as tanks, planes, or ships.

Just like LLNL's TSAR software described above, MGED was developed for use on workstations with high-resolution graphics that use UNIX operating systems. As opposed to TSAR, the entire MGED code is written in the "C" programming language. The most recent distribution of BRL-CAD features Version 4.0 of the code. This software, which was obtained for evaluation at NRaD and University of South Carolina, and installed on the Silicon Graphics IRIS 4-D workstation, was used to create several scattering objects for FD-TD simulations reported on in the next section.

The user interface of BRL-CAD is intended for an "expert user" rather than for a novice who needs a "user-friendly" software package. However, even someone without extensive knowledge of solid model building could use this software effectively as well. Simple objects such as plates or combinations of plates and wires were created following a half-day's work, with the help of Applin et al. (1988).

It should be pointed out that the five-volume documentation package that includes the user's manual, which came with the distribution of Version 4.0 software, is really useful. Numerous examples are included with step-by-step instructions and pictures of many editing functions. In addition, BRL-CAD also comes with sample files discussed in the manual. The developers of the software have invested considerable effort into providing "readable" and "understandable" documentation.

MGED has one drawback. To take advantage of the graphical capabilities of computer workstations, it was naturally designed for the UNIX operating systems. Unfortunately, the implementation of UNIX operating systems varies from one manufacturer to another. In addition, there are also several different operating system standards (Berkeley and AT&T). The developers have ported BRL-CAD to many different UNIX platforms in the attempt to update the software to conform with the latest 05 upgrades. However, the frequency of system upgrades many times outpaces the most recent version of MGED. As a result, the best way to take full advantage of MGED is to stay with a single version of the operating system for as long as possible until the new "patch" to the software becomes available from BRL.

3.0 NUMERICAL RESULTS

This section concentrates on the numerical results obtained from FD-TD runs for several scattering and radiation geometries. Specifically, the scattering studies were performed for grounded perfectly conducting wires and plates, as well as for lossy dielectric plates. The interest in such structures stems partly from using FD-TD as a numerical validation or as a calibration tool for data measured on NRaD's time-domain range. In addition, these results can also serve to validate the method of moments codes such as JUNCTION and MOSAIC developed at the University of Houston (Wilton & Hwu, 1988).

3.1 SCATTERING AND RADIATION FROM GROUNDED WIRE ANTENNAS

Consider a grounded, perfectly conducting, and *y*-directed 30-cm-long monopole antenna (figure 5) with a square cross-section of 1 cm x 1 cm. This geometry is one example that comes with TSAR distribution. The excitation to the wire is in the form of a *y*-polarized plane wave whose time dependence is a narrow Gaussian pulse.

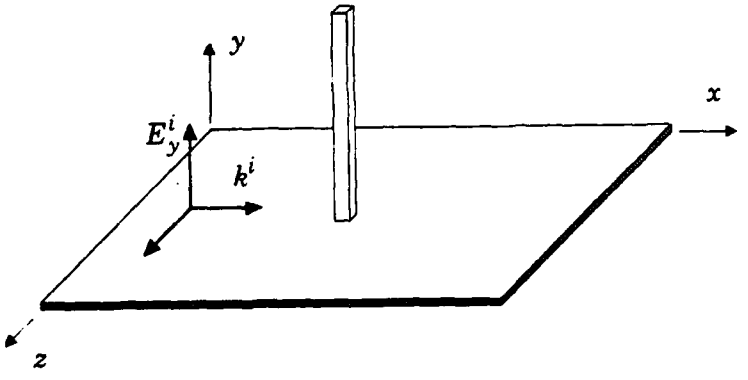

Figure 5. Grounded copper monopole excited by a plane wave.

Both the excitation and the induced current density at the base of the wire are shown in figure 6. Note that as expected from physical optics, the peak of the current density reaches 2 *A/m*, indicating that TSAR predicts proper physical response of the wire. Since FD-TD can produce a wealth of data with every single run, the current density was also recorded half-way between the wire base and its tip. Once again, the proper physical optics peak current density value was predicted by FD-TD code (figure 7). To complete the scattering study from the copper wire, the total *y*-directed electric field was computed 5 cm in front of as well as behind the wire (figure 8), which demonstrates the flexibility of TSAR to provide total field data anywhere within the computational space.

Next, to examine the ability of TSAR to calculate the induced current density at several points on the same 30-cm monopole, a delta-gap generator operating at 1 GHz was placed between the ground plane and the base of the wire to provide the transient excitation. For simplicity, the magnitude of the applied voltage source was taken to be 1 V, and its time waveform was assumed to be a short Gaussian pulse. This form of excitation was modeled by TSAR by

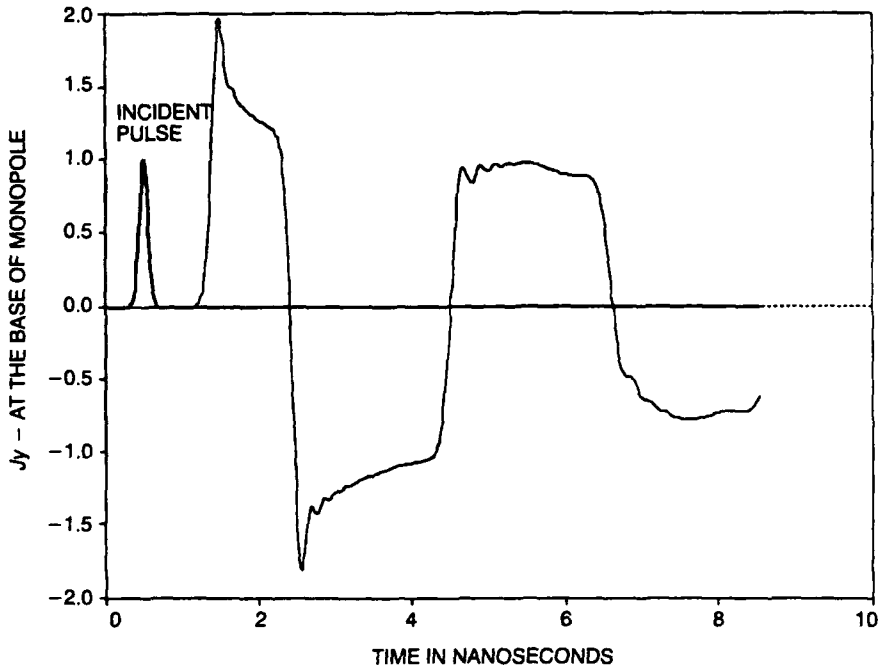

Figure 6. Induced surface current density (A/m) at the base of a grounded monopole.

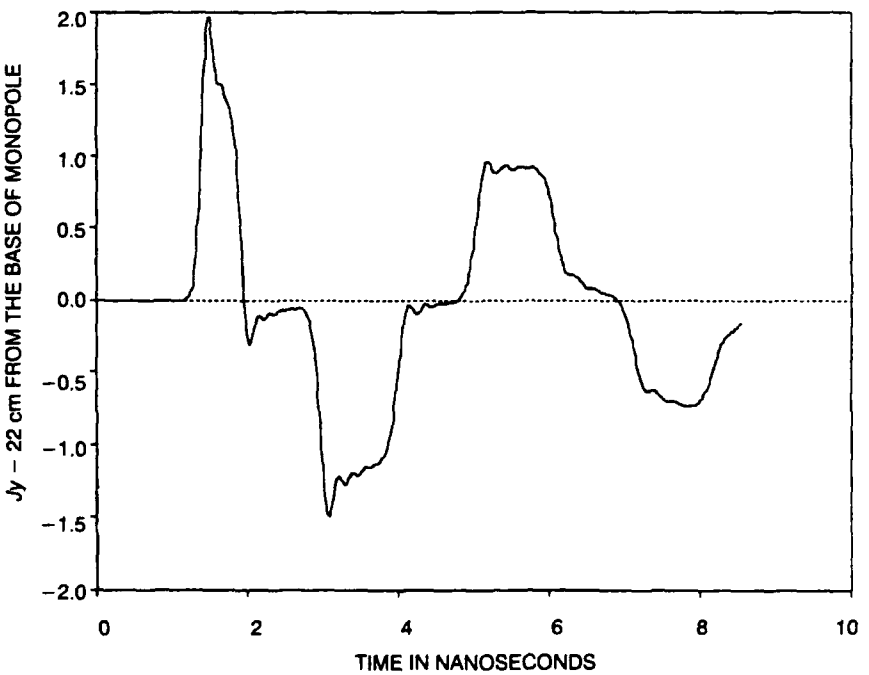

Figure 7. Induced surface current density (A/m) 15 cm from the base of a grounded monopole.

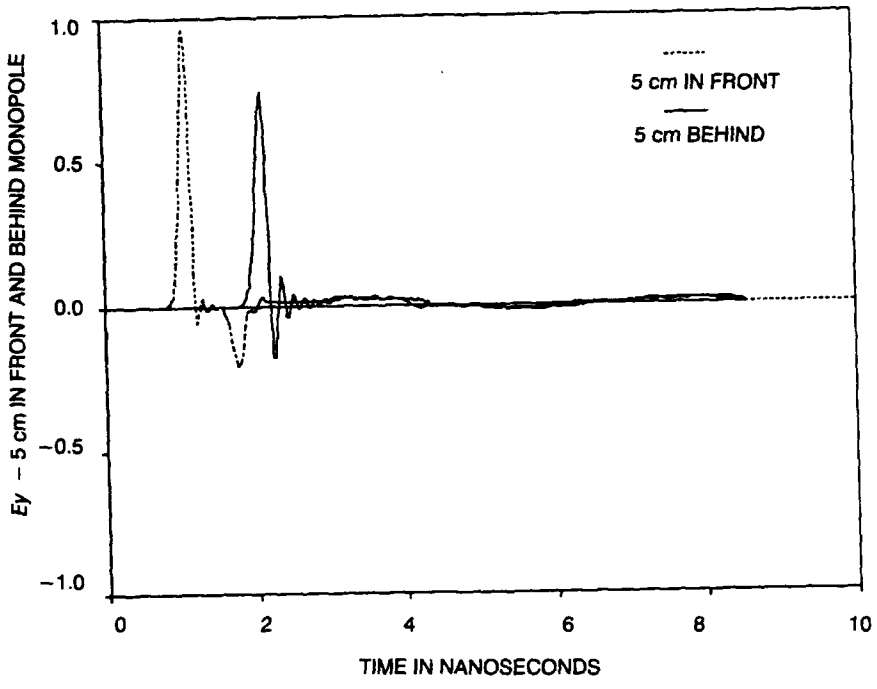

Figure 8. Y-component of E-field (V/m) 5 cm in front and behind a grounded monopole.

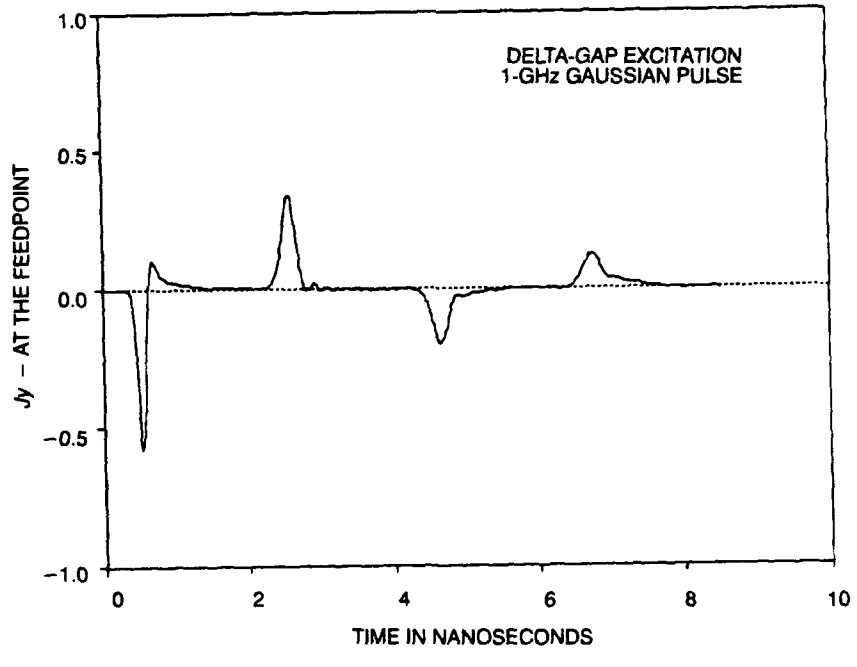

Figure 9. Induced surface current density (A/m) at the feed point of a grounded monopole.

defining a y-directed point radiator at the first cell above the perfectly conducting ground plane. Finally, it should be added that in both scattering examples presented above, and in the following radiation runs, the wire was modeled as a copper conductor having large but finite conductivity.

Figures 10 through 13 show the y-component of $\bar{J}$ at various locations on the wire as functions of time. Notice that TSAR yields the time history of the surface current density (in A/m rather than volume current density in A/m^2), which is different at each location. This is due to interference between the signal generated at the feed and its reflections from the wire tip, as well as the ground plane upon the current wave's return from the tip. The total transit time for the pulse to propagate the length of the wire is 2 ns. As illustrated in figure 10, the surface current density 7 cm above the ground plane "feels" the excitation shortly after it is applied, and experiences the effects of the reflection from the tip 2 ns later, followed by the effects of ground reflection soon after. This is illustrated in figure 10 by two adjacent peaks at time $t = 2$ ns. The first of these two peaks is due to the reflection from the tip, while the second corresponds to the reflection from the ground plane. Similar results can also be observed from figures 11 to 13 for the surface current density at other locations on the wire

TSAR's implementation of FD-TD was also evaluated in calculation of the wire radiation characteristics, such as in predicting its input impedance. The time-domain waveform of the excitation voltage in the gap was taken to be a sinusoid at a frequency of 250 MHz. The induced surface current density flowing on the antenna right next to the gap is shown in figure 14. As seen from the plot, J_y builds up to its steady-state value gradually after 15 ns. Once the surface current density has reached its steady-state value, the real part of the input impedance of the wire antenna may be calculated from the computed data by using the following equation:

$$R(\Omega) = \frac{V_{gap}(V)}{I_{peak}(A)} = \frac{1V}{\left(J_y(A/m)\cdot \Delta y(cm)/100\right)} \quad , \tag{4}$$

provided that the segment length is specified in centimeters. For the example shown in figure 14, for the peak surface current density of 2.2 A/m, the resistive part of input impedance of the monopole antenna is given by

$$R = \frac{V_{gap}}{I_{peak}} = \frac{1V}{(2.2/100)A} = 45.5\Omega \tag{5}$$

compared to 49Ω, which was calculated with MININEC (Logan & Rockway, 1986) at the same frequency and the equivalent radius of 0.59 cm (King, 1956).

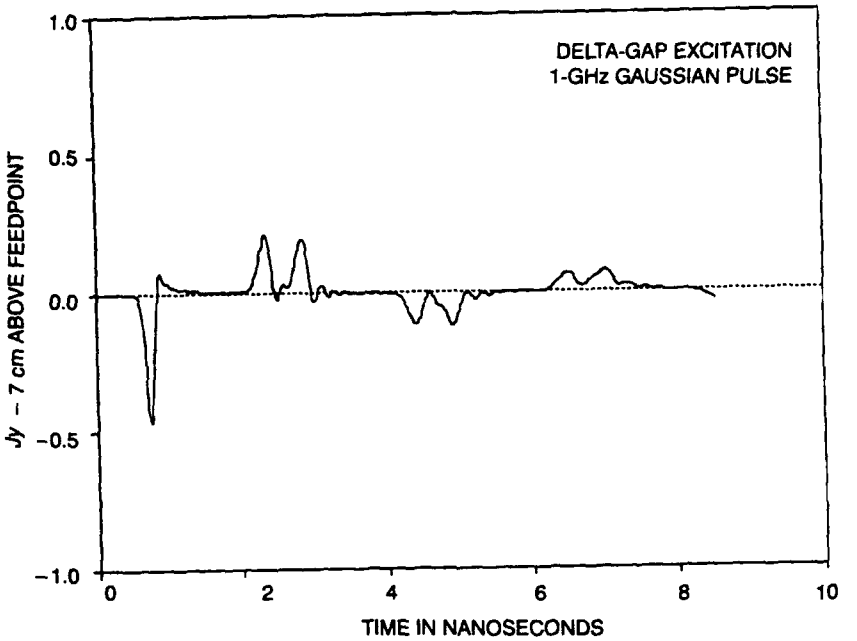

Figure 10. Induced surface current density (A/m) 7 cm above feed of a grounded monopole.

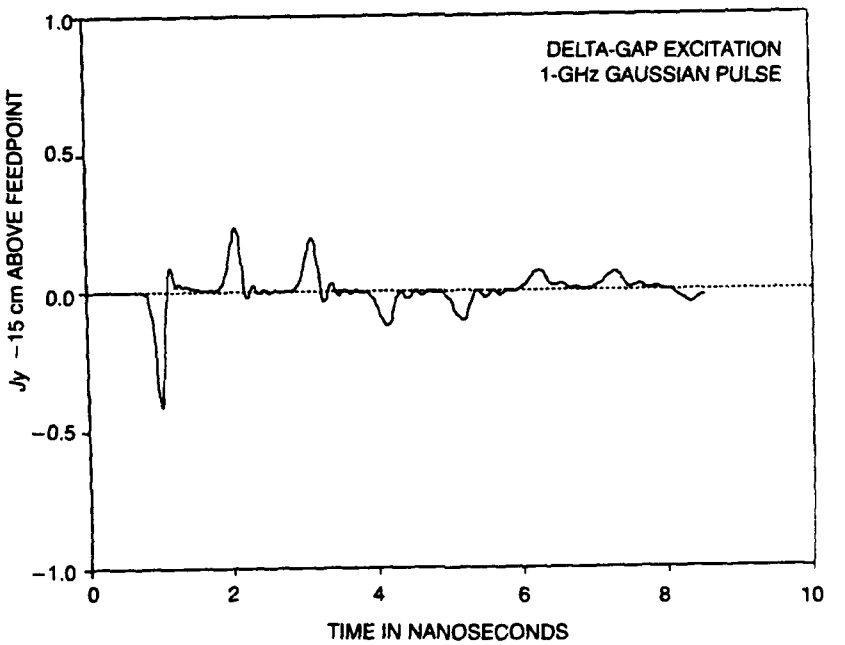

Figure 11. Induced surface current density (A/m) 15 cm above feed of a grounded monopole.

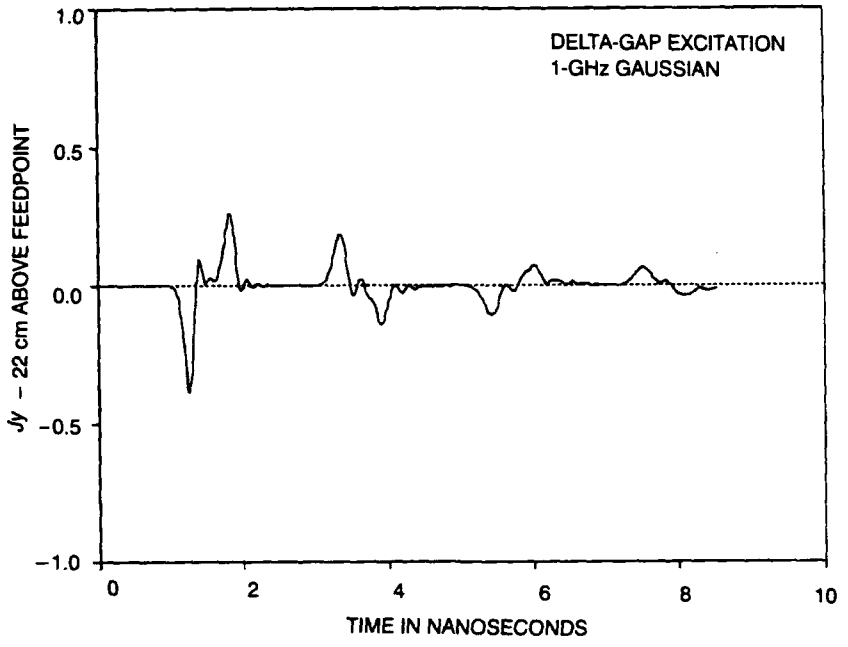

Figure 12. Induced surface current density (A/m) 22 cm above feed of a grounded monopole.

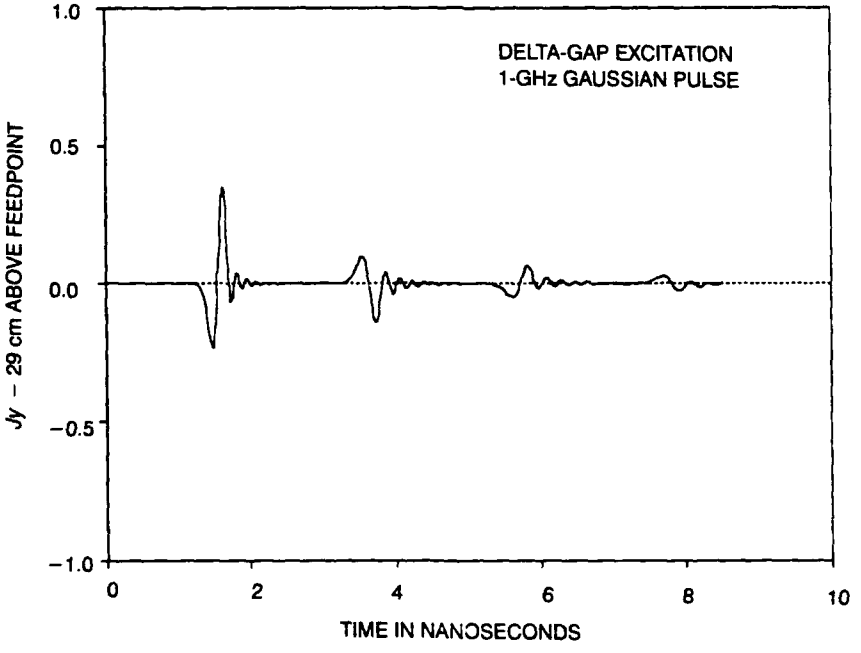

Figure 13. Induced surface current density (A/m) 29 cm above feed of a grounded monopole.

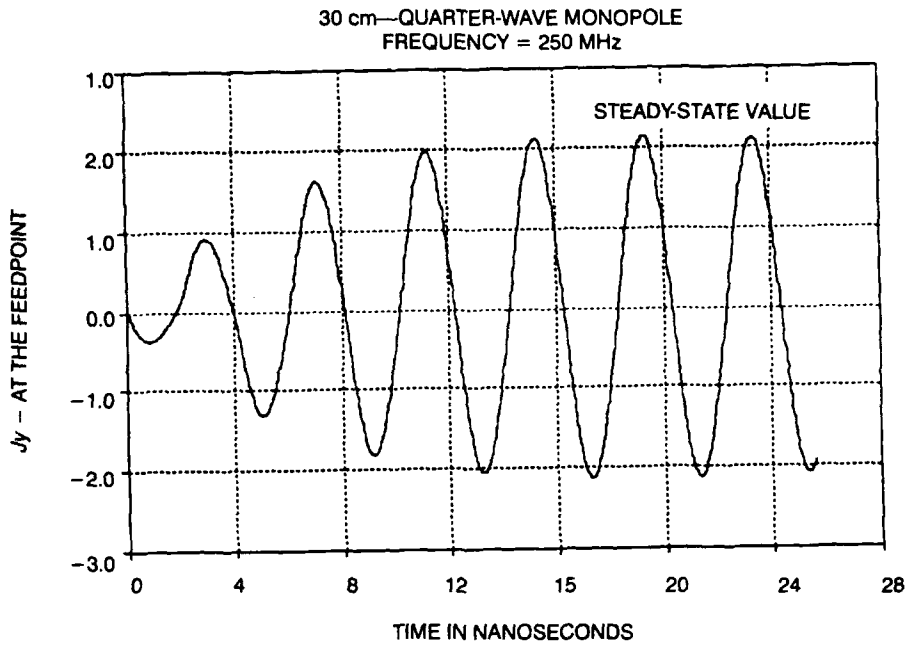

Figure 14. Induced surface current density (A/m) at the feed of a grounded monopole.

3.2. SCATTERING FROM GROUNDED METALLIC PLATES

To evaluate FD-TD's potential use as the time-domain range or target calibration tool, numerical scattering studies from a grounded metallic plate were carried out. Figure 15 shows the plate geometry and the polarization of the incident plane wave.

Although the scattering geometry of figure 15 is an idealization of the actual experimental setup, it can nevertheless provide an accurate approximation to what happens in practice. Structural flaws of the range (seams or large cracks), interference due to the surroundings, equipment malfunctions, or errors in signal processing algorithms can be detected by making comparison of measured and calculated data.

In addition to detecting potential problems with the range and measurement procedure, FD-TD can also be exploited as a time-domain reference target calibration tool. Numerical construction (or generation) of the target geometry on the computer is simpler and more cost effective than building the prototype. This is especially true when the realistic target shapes are needed. Hence, the numerical results simulated with FD-TD for a realistic reference target may be used to replace the measured signature of the prototype.

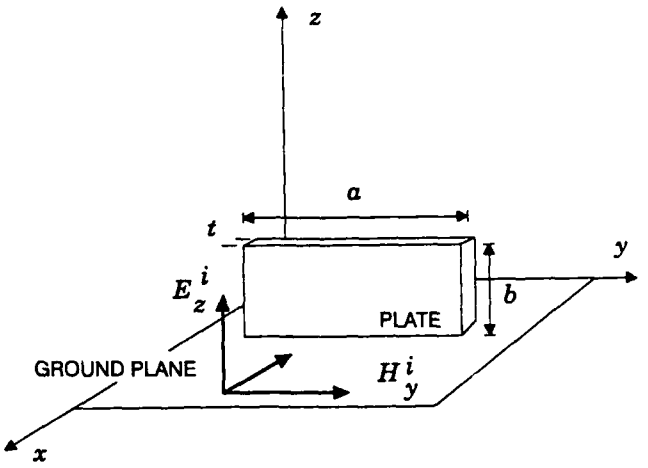

Figure 15. Geometry of a grounded perfectly conducting plate excited by a plane wave.

To compute scattering data presented in this section, a double exponential pulse with 120-ps risetime and 1-ns falltime was used to illuminate the grounded plate (figure 16). Figure 17 contains the plot of the surface current density at the center of the plate, which is placed with its narrow side (a = 15 cm) on the ground and its long side (b = 24 cm) exposed to the excitation. As can be seen, the long duration of the excitation in time and this particular orientation of the plate cause considerable ringing in the induced surface current density.

In addition to the surface current computations, the total electric field was also obtained from the same FD-TD runs. Figure 18 displays the z-component of the electric field 5 cm in front of, as well as 5 cm behind, the plate. Notice that the field in front of the plate (dotted line in figure 18) illustrates the interaction of the incident and reflected field components. The time history of E_z at that location initially shows the propagating incident field building up to its maximum value of 1.0 V/m. Then approximately at 0.5 ns, the reflection takes place and the incident field is nearly canceled by the oppositely polarized reflected field. This is subsequently followed by a gradual buildup of the total field due to further interference of the incident and reflected fields.

Next, the same plate was placed on the ground plane along its wide dimension (a = 24 cm) with its short side (b = 15 cm) exposed to the electric field of the incident wave. The time dependence of the excitation was assumed to be the same double exponential pulse (figure 16). The surface current density induced at the center of the plate is shown in figure 19. As opposed to the results for the current density at the center of the tall plate (figure 17), the ringing in J_z of the short plate is significantly lower. Such behavior is physically reasonable and can be associated with different plate resonances.

For the short conducting plate, figure 20 shows the z-component of the total electric field 5 cm in front of and 5 cm behind the plate. In this case, the E-field displays similar properties observed earlier for the tall plate (figure 18). These results suggest that the orientation of the plate appears to produce minor differences in the fields close to the structure despite having significantly different induced current densities. This behavior can be attributed to magnitude rather than phase effects dominating the nature of the field in the near zone.

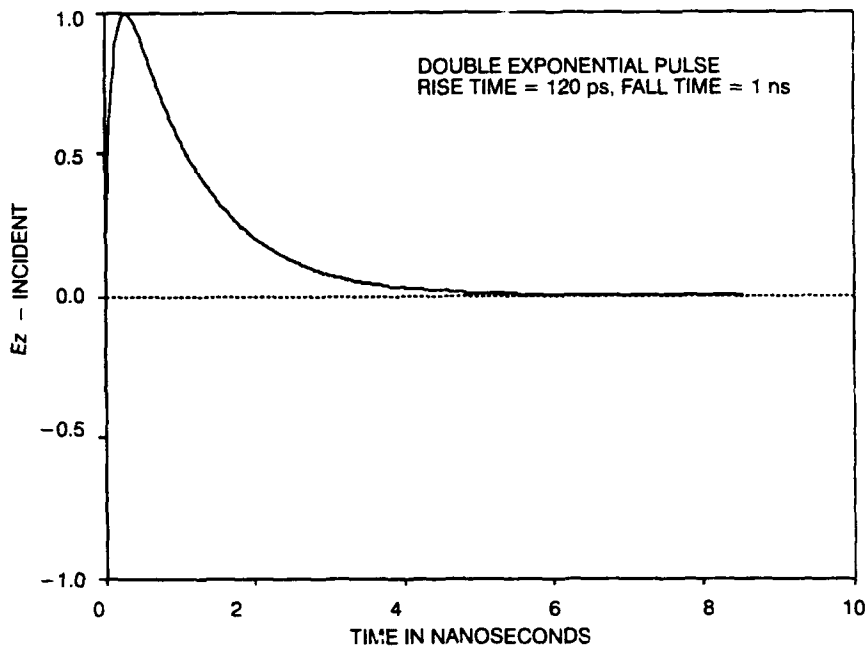

Figure 16. An EMP pulse incident on a grounded metal or dielectric plate.

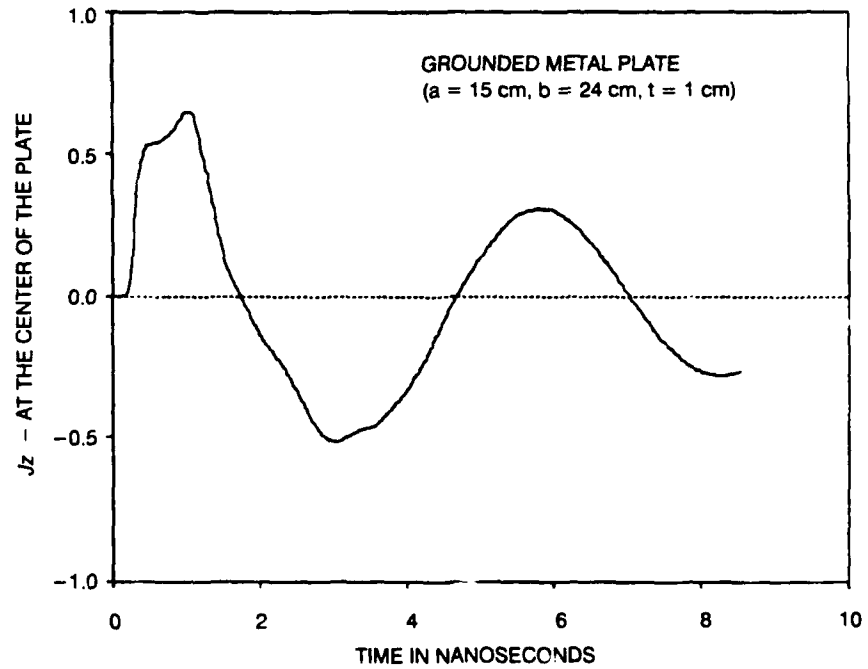

Figure 17. Induced surface current density (A/m) at the center of a grounded metal plate.

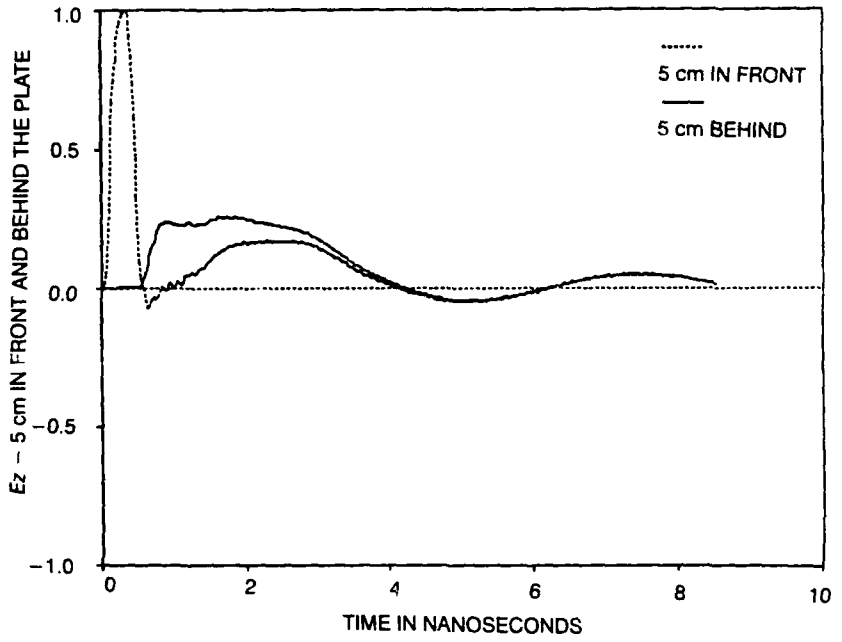

Figure 18. Z-component of E-field (V/m) 5 cm in front and behind a grounded metal plate.

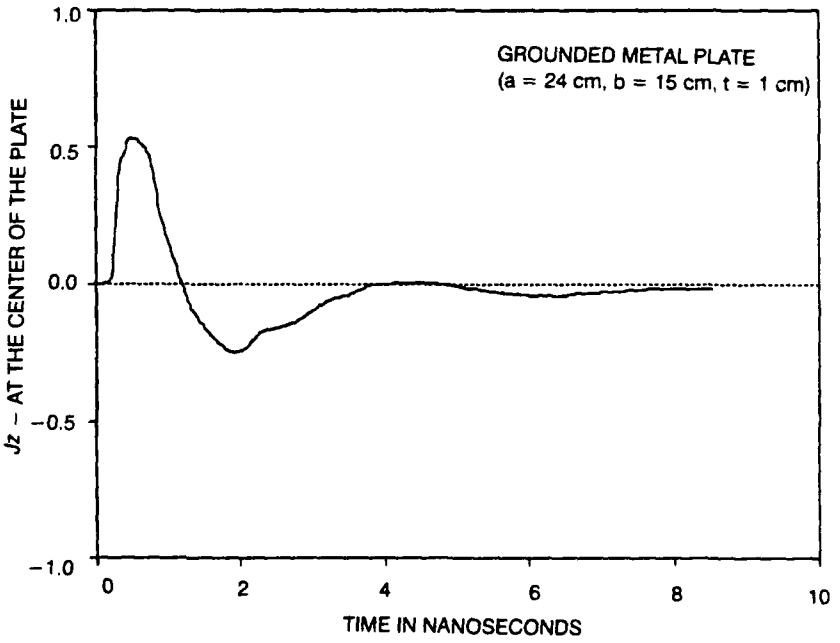

Figure 19. Induced surface current density (A/m) at the center of a grounded metal plate.

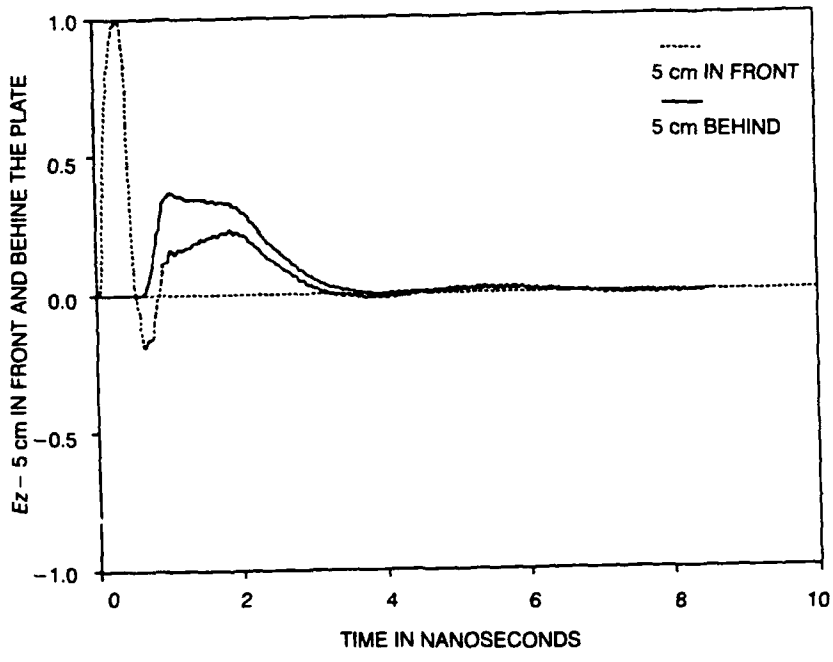

Figure 20. Z-component of E-field (V/m) 5 cm in front and behind a grounded metal plate.

3.3. SCATTERING FROM GROUNDED LOSSY DIELECTRIC PLATES

The final set of data represent time-domain scattering from penetrable material plates. Figures 21 through 23 show comparisons between grounded lossless and lossy dielectric plates. The relative dielectric constant, ε_r, used in these studies is 5. The excitation is still assumed to be in the form of the z-polarized double exponential pulse (figure 16), whose frequency is 1 GHz. Physical dimensions of the plate a, b, and t are 24, 15, and 1 cm, respectively.

The time history of the tangential component of the electric field (namely, E_z) was recorded at the center of the plate. As seen from figure 21, the two curves that correspond to lossless (solid line) and lossy (dotted line) plates are nearly the same. The primary effect of finite conductivity appears to be a slight reduction of the field level. Notice that in either case, once the incident field passes through the plate, a considerable amount of ringing takes place due to internal reflections within the plate interacting with the incident field. The ringing is present in both lossy and lossless plates, though its level is lower in the lossy plate due to dissipation.

Next, the z-component of the total E-field is displayed in figure 22. Initially, it shows the incident pulse passing through the point of observation. However, at approximately 0.5 ns, the reflected wave arrives and begins to interact with the trailing edge of the excitation. As opposed to the metal plate, where the reflection coefficient is equal to negative 1, only a fraction of the incident field is reflected from the dielectric plate. As a result, the total field level is higher in front of the dielectric plate as compared to its metallic counterpart (figure 18 or 20).

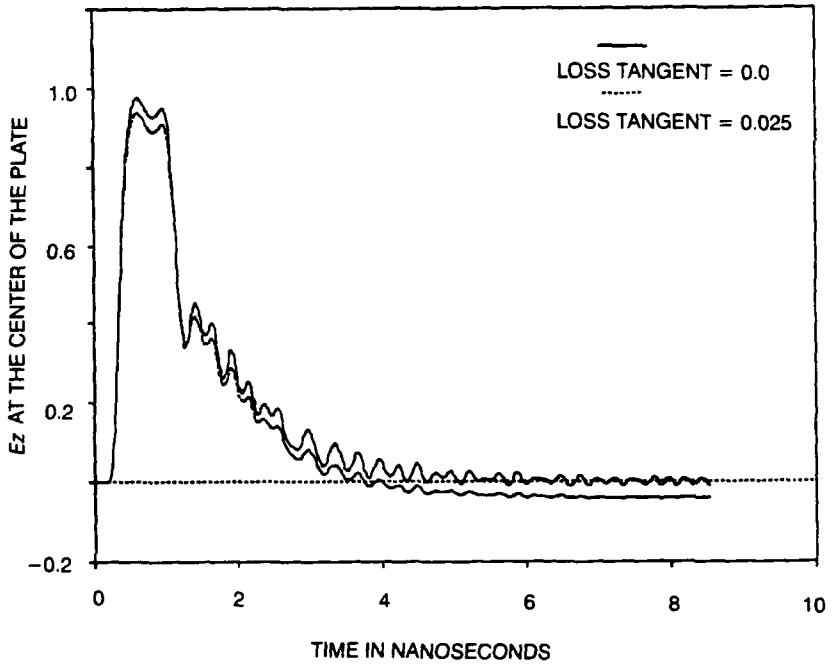

Figure 21. Z-component of *E*-field (V/m) at the center of a grounded dielectric plate.

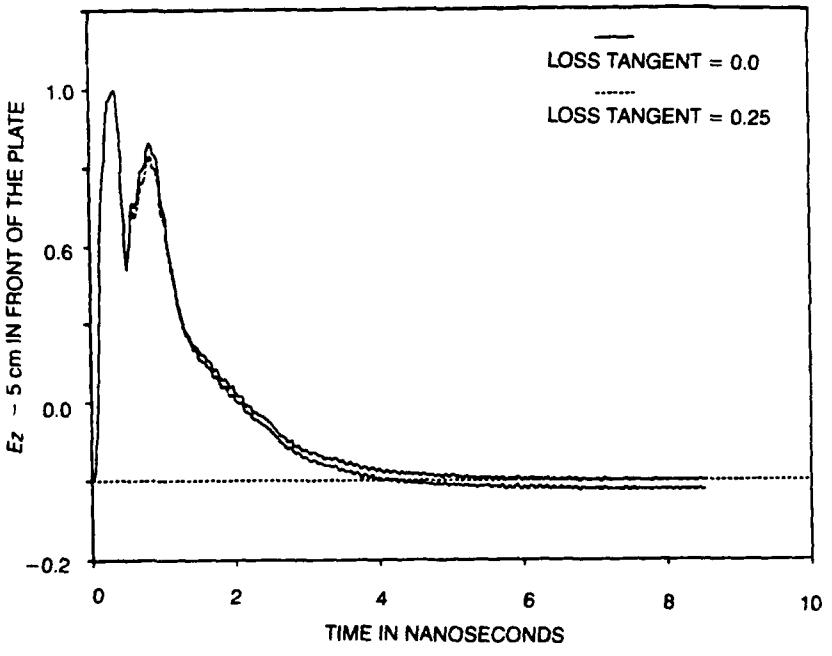

Figure 22. Z-component of *E*-field (V/m) 5 cm in front of a grounded dielectric plate.

Finally, figure 23 contains the plots of z-components of the total electric field 5 cm behind the dielectric plate, as well as the replica of the incident wave. An interesting observation may be made from this figure. Notice that the total field level for both lossy and lossless plates exceeds that of the excitation. In addition, the field behind the plate also retains practically the same time-domain shape as that of the incident field. These results suggest that the incident field is reinforced by internal reflections from the internal boundaries of the plate. The level of such reinforcement depends on the thickness of the plate as well as on its electrical properties.

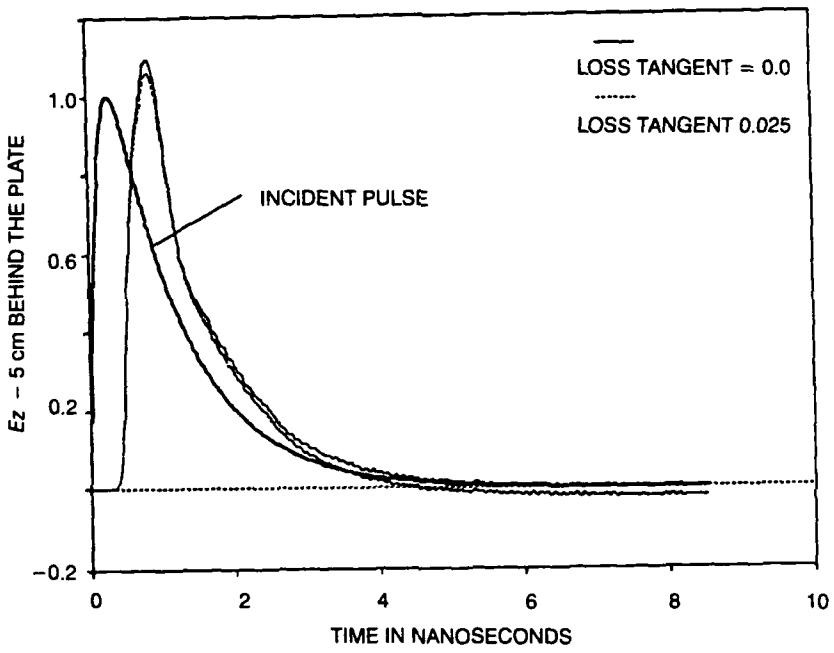

Figure 23. Z-component of E-field (V/m) 5 cm behind the grounded dielectric plate.

4.0 SUMMARY

The use of the FD-TD method was examined in the scattering and radiation problems of interest to the Navy. Several numerical case studies were carried out by using the TSAR code with the numerical implementation of FD-TD developed at the LLNL. This package was made available by LLNL to NRaD and to the University of South Carolina for this study.

The TSAR software and its associated utilities were evaluated for ease of use and flexibility to analyze complex EM interaction problems. TSAR was found to be a very powerful numerical modeling tool. In general, TSAR is not difficult to use. However, it will take the user some time to learn how to take full advantage of this code. TSAR requires familiarity with FD-TD; basic knowledge is sufficient.

Numerical studies included time-domain radiation and scattering from grounded thin wires. Induced surface currents were computed on the wire, and electric fields were calculated in its vicinity. It was found that FD-TD provides a wealth of data about the electromagnetic interaction of the incident field with its surroundings. Both currents and fields may be calculated everywhere in the region of interest with a single run of the TSAR code.

In addition, FD-TD was effective in predicting radiation characteristics of wire antennas including calculation of antenna impedance. Despite FD-TD's modeling of the wire cross-section as square rather than circular, accurate input impedance values were obtained when compared to the results computed with MININEC. This suggests that with proper modifications that include conformal grids, precise values of wire impedances can be calculated with FD-TD.

Finally, FD-TD was employed to investigate the scattering properties of grounded metallic, lossless, and lossy dielectric plates. The FD-TD was used to verify experimental observations made on NRaD's time-domain range. The calculated data showed similar field behavior to that obtained through measurements. In this capacity, FD-TD can serve as a numerical target or range calibration tool.

5.0 REFERENCES

Applin, K. A., M. J. Muus, R. J. Reshley, M. Gigante, and I. Overend. 1988 "User's Manual for BRL-CAD Graphics Editor," Ballistic Research Laboratory (October), Aberdeen Proving Ground, MD.

Applin, K A., M. J. Muus, R. J. Reshley, M. Gigante, and I. Overend. 1991 "The Ballistic Research Laboratory CAD Package Release 4.0," Ballistic Research Laboratory (December), Aberdeen Proving Ground, Md.

Beker, B., K. R. Umashankar, and A. Taflove. 1989. "Numerical Analysis and Validation on the Combined Surface Integral Equations for Electromagnetic Scattering by Two-Dimensional Anisotropic Objects," *IEEE Trans. Antennas Prop.*, vol. AP-37, no. 12, pp. 1573–1581 (December).

Beker, B. 1992. "Application of Integral and Differential for Various EM Equation Methods Interaction Problems," NRaD TD 2453 (August), San Diego, CA.

Graglia, R. D., and P. L. E. Uslenghi. 1987. "Electromagnetic Scattering from Anisotropic Materials, Part II: Computer Code and Numerical Results in Two-Dimensions," *IEEE Trans. Antennas Prop.*, vol. AP-35, no. 2, pp. 225–232 (February).

Harrington, R. F. 1968. *Field Computation By Moment Methods*, The MacMillan Company, New York, NY.

Kashyap, S., M. Burton, and A. Louie. 1992. "EM Field Penetration Inside the Bridge of a Ship," *IEEE AP-S International Sym. Digest*, vol. 3, pp. 1694–1697 (July).

King, R. W. P. 1956. *The Theory of Linear Antennas*, p. 20, Harvard University Press, Cambridge, MA.

Laguna, G. 1990. "Anastasia: A Solid Model Based 3D Finite Difference Mesh Generator," UCRL-MA-105580, Lawrence Livermore National Laboratory (November), Livermore, CA.

Logan, J. C., and J. W. Rockway. 1986. "The New MININEC (Version 3.0): A MiniNumerical Electromagnetic Code," NOSC TD 938, Naval Ocean Systems Center (September), San Diego, CA.

Luebbers, R. J., K S. Kunz, M Schnieder, and F. Hunsberger. 1991. "A Finite-Difference Time-Domain Near Zone to Far Zone Transformation," *IEEE Trans. Antennas Prop.*, vol. AP-39, no. 4, pp. 429–433 (April).

McLeod, R. R. 1990. "Temporal Scattering and Response Software," UCRL-MA 104861, Lawrence Livermore National Laboratory (September), Livermore, CA.

McLeod, R. R. 1992. "Temporal Scattering and Response Software Users' Manual Version 2.3," UCRL-MA 104861 V 2.3, Lawrence Livermore National Laboratory (June), Livermore, CA.

McLeod, R. R., and M. J. Allison. 1990. "IMAGE 3.3 Tutorial Manual," UCR-MA 104860, Lawrence Livermore National Laboratory (October), Livermore, CA.

Monzon, J. C. 1988. "On a Surface Integral Representation for Homogeneous Anisotropic Regions: Two-Dimensional Case," *IEEE Trans. Antennas Prop.*, vol. AP-36, no. 10, pp. 1401–1406 (October).

Mur, G. 1981. "Absorbing Boundary Conditions for the Finite Difference Approximation of Time Domain Electromagnetic Field Equations," *IEEE Trans. Electromagn. Compat.*, vol, EMC-23, pp. 377–382.

Taflove, A. 1988. "Review of the Formulation and Applications of the Finite-Difference Time-Domain Method for Numerical Modeling of Electromagnetic Wave Interactions with Arbitrary Structures," *Wave Motion*, vol. 10, pp. 547–582 (December).

Taflove, A., and K. R. Umashankar. 1987. "Advanced Numerical Modeling of Microwave Penetration and Coupling for Complex Structures," UCRL-15960, Lawrence Livermore National Laboratory, Livermore, CA.

Umashankar, K. R., and A. Taflove. 1982. "A Novel Method to Analyze Electromagnetic Scattering by Complex Objects," *IEEE Trans. Electromagn. Compat.*, vol. EMC-24, pp. 397–405.

Wilton, D. R., and S. U. Hwu. 1988. "Junction Code User's Manual: Electromagnetic Scattering and Radiation by Arbitrary Configurations of Conducting Bodies and Wires, "NOSC TD 1324, Naval Ocean Systems Center (December), San Diego, CA.

Yee, K S. 1966. "Numerical Solution of Initial Boundary Value Problems Involving Maxwell's Equations in Isotropic Media," *IEEE Trans. Antennas* Prop., vol. AlS-12, no. 3, pp. 302–307, May.

6.0 ACRONYMS

BRL	Ballistic Research Laboratory
EM	electromagnetic
FD-TD	finite-difference time-domain
LLNL	Lawrence Livermore National Laboratory
MGED	multidevice graphics editor
MOM	method of moments
OS	operating system
TSAR	temporal scattering response

REPORT DOCUMENTATION PAGE

Form Approved
OMB No. 0704-0188

1. AGENCY USE ONLY *(Leave blank)*	2. REPORT DATE	3. REPORT TYPE AND DATES COVERED
	December 1992	Final

4. TITLE AND SUBTITLE
APPLICATION OF THE FINITE-DIFFERENCE TIME-DOMAIN METHOD TO SCATTERING AND RADIATION PROBLEMS INVOLVING WIRES AND PLATES

5. FUNDING NUMBERS
PE: 0602121N
WU: DN088509

6. AUTHOR(S)
B. Beker, College of Engineering, University of South Carolina

7. PERFORMING ORGANIZATION NAME(S) AND ADDRESS(ES)
Naval Command, Control and Ocean Surveillance Center (NCCOSC)
RDT&E Division
San Diego, CA 92152-5000

8. PERFORMING ORGANIZATION REPORT NUMBER
TD 2516

9. SPONSORING/MONITORING AGENCY NAME(S) AND ADDRESS(ES)
Office of Naval Technology
Arlington, VA 22217-5000

10. SPONSORING/MONITORING AGENCY REPORT NUMBER

11. SUPPLEMENTARY NOTES

12a. DISTRIBUTION/AVAILABILITY STATEMENT
Approved for public release; distribution is unlimited.

12b. DISTRIBUTION CODE

13. ABSTRACT *(Maximum 200 words)*

This report reviews the application of the finite-difference time-domain (FD-TD) method to problems dealing with interaction of electromagnetic (EM) fields with wires, plates, and other three-dimensional scattering geometries. Selection of finite-difference time-domain (FD-TD) for this study was motivated primarily by its generality and its ability to treat a very wide of class time-domain scattering problems. The temporal scattering and response (TSAR) code was made available for evaluation by the Lawrence Livermore National Laboratory to NRaD and to the University of South Carolina. The TSAR software was used to analyze transient scattering and radiation from wire antennas as well as scattering from metallic and dielectric plates. The evaluation of the code and its associated pre- and post-processing utilities was based on the ease of use, clarity of software description in the manuals, and ability to solve electromagnetic time-domain interaction problems of interest to the Navy.

14. SUBJECT TERMS
electromagnetic interaction problems
temporal scattering and response code
multidevice graphics editor

15. NUMBER OF PAGES
36

16. PRICE CODE

17. SECURITY CLASSIFICATION OF REPORT	18. SECURITY CLASSIFICATION OF THIS PAGE	19. SECURITY CLASSIFICATION OF ABSTRACT	20. LIMITATION OF ABSTRACT
UNCLASSIFIED	UNCLASSIFIED	UNCLASSIFIED	SAME AS REPORT

21a. NAME OF RESPONSIBLE INDIVIDUAL	21b. TELEPHONE *(include Area Code)*	21c. OFFICE SYMBOL
B. Beker	(619) 553–5089	Code 822

INITIAL DISTRIBUTION

Code 0012	Patent Counsel	(1)
Code 0141	A. Gordon	(1)
Code 80	K. D. Regan	(1)
Code 805	J. W. Rockway	(1)
Code 82	R. J. Kochanski	(1)
Code 824	J. B. Rhode	(1)
Code 824	C. A. Deneris	(1)
Code 824	J. Ho	(1)
Code 824	L. B. Koyama	(1)
Code 824	S. T. Li	(1)
Code 824	J. C. Logan	(10)
Code 824	A. Page	(1)
Code 824	L. C. Russell	(1)
Code 824	J. H. Schukantz	(1)
Code 824	D. W. Tam	(1)
Code 961	Archive/Stock	(6)
Code 964B	Library	(2)

Defense Technical Information Center
Alexandria, VA 22304–6145 (4)

NCCOSC Washington Liaison Office
Washington, DC 20363–5100

Center for Naval Analyses
Alexandria, VA 22302–0268

Navy Acquisition, Research and Development
Information Center (NARDIC)
Washington, DC 20360–5000

GIDEP Operations Center
Corona, CA 91718–8000

NCCOSC Division Detachment
Warminster, PA 18974–5000

Space and Naval Warfare Systems Command
2451 Crystal Drive
Arlington, VA 22245–5200 (4)

Naval Sea Systems Command
Washington, DC 20362–5101 (2)

Office of Naval Research
Arlington, VA 22217–5000

Naval Surface Warfare Center
Carderock Division
Bethesda, MD 20084–5000

Naval Postgraduate School
Monterey, CA 93940

U.S. Army Information Systems Eng
and Integration Center
Fort Huachuca, AZ 85613–7300

The University of South Carolina
Columbia, SC 29208 (10)